Numerical simulation of sine-Gordon soliton dynamics in the presence of perturbations*

J. F. Currie, S. E. Trullinger,† A. R. Bishop,‡ and J. A. Krumhansl
Laboratory of Atomic and Solid State Physics and Materials Science Center, Cornell University, Ithaca, New York 14853
(Received 20 December 1976)

We have developed a computer simulation program to study the dynamical behavior of soliton solutions of the sine-Gordon equation in the presence of external perturbations. Our work extends numerical and formal mathematical analysis on the sine-Gordon system in four directions. First, we demonstrate that lossless soliton propagation on a lattice is complicated by a lattice pinning effect and the generation of "harmonic excitations" as "radiation." We define regimes according to the coefficient ω_0^2 of the nonlinear potential term in which propagation can ($\omega_0^2 \lesssim 1$) or cannot ($\omega_0^2 \gtrsim 1$) occur. Second, we study two examples of perturbation which are of particular importance in condensed matter: (i) a model impurity binds low-velocity solitons but merely space shifts those with high velocities, and (ii) spatial inhomogeneities in the coefficient of the nonlinear term ω_0^2 cause the soliton to adjust its velocity and shape in the regions of imperfection. We find that the results of Fogel *et al.*, who treat these types of perturbation in a linear perturbation theory, are accurate to better than 25% as long as the small parameter does not exceed 0.1. Third we demonstrate that their conclusion that solitons can be treated as classical φ particles obeying Newton's laws is in excellent agreement with the simulation results. Finally we indicate several applications of our simulation results for the propagation of a quantum of flux along a Josephson-junction transmission line.

I. INTRODUCTION

The sine-Gordon partial differential wave equation has been widely studied by mathematicians and physicists due to not only its complete integrability and accompanying remarkable "soliton" properties but also its ubiquity as a model of nonlinear physical phenomena.[1] Its kinklike solitary wave solution has been used to describe excitations in many areas of condensed matter physics, to name a few, domain walls in ferromagnets,[2] dislocations in crystals,[3] charge carriers in one-dimensional Fröhlich charge-density-wave condensates[4] and flux quanta on Josephson-junction transmission lines.[5] In order to understand soliton dynamics in systems of practical interest, it is necessary to know how the soliton interacts with spatial inhomogeneities (e.g., due to impurities or defects) and with external forces. Moreover, for networks and systems in which there are natural minimum distance scales such as an underlying crystal lattice, discreteness effects may significantly modify the continuum dynamics described by the sine-Gordon equation.

Recently it has become possible to treat perturbations and discrete chain problems analytically. Fogel, Trullinger, Bishop, and Krumhansl[6] (hereafter I) starting from certain initial conditions used a linear perturbation scheme to investigate, first, model spatial inhomogeneities in the coefficient of the nonlinear term in the sine-Gordon equation, and second, two external forces: a two-point impulsive force, and an external driving force (static or time dependent) with damping. They found that in many respects the soliton behaved in the presence of weak perturbations as a deformable extended particle governed by Newton's laws. Although their method has the advantage of applying naturally to a general class of solitary-wave-bearing equations, it is impractical for perturbation with respect to multisoliton solutions. Kaup and Newell[7] have extended the inverse scattering transform, to treat deviations from fully integrable systems. In the present context they have confirmed[8] the (in fact "relativistic") particle behavior reported in I and also treated[9] the effects of an external driving force with damping on a "breather" or "doublet" solution (soliton-antisoliton bound state). Keener and McLaughlin[10] have also developed a perturbation formalism which employs a Green's-function technique and, as with the latter approach, can in principle be used to treat general multisoliton solutions. All of the above methods are only practical, however, for small numbers of solitons. The external static driving force with damping has also been treated using numerical solutions by Scott, Chu, and Reible.[11] For few solitons they use the inverse scattering formalism while for many solitons they use Whitham's averaged Lagrangian analysis[12] in order to calculate numerically the evolution of the multisoliton solution for arbitrary forces and dampings. Nakajima *et al.* have performed simulations of soliton propagation and collisions, both mechanically[13] and numerically,[14,15] again for static driving forces and damping. Simulation of sine-Gordon soliton collisions by Ablowitz *et al.*[16] seems to be the first report of "radiation" due to discreteness effects in the sine-Gordon problem.

Some experimental work[11,17] has been possible

regarding the propagation of fluxons along Josephson-junction transmission lines. These studies are difficult to conduct and control. Numerical simulations on the other hand offer a realistic and inexpensive means of examining propagation relatively easily.

Although of very general mathematical and physical interest, much of the work to date has been motivated by the possibility of applying flux propagation along a Josephson-junction transmission line to the development of high-speed, high-density, and low-power memory and logic devices.[18] On the basis of the above work, logic device designs have been proposed.[19,20] For technical reasons junction logic devices appear likely to be constructed as arrays of discrete junctions so that the discreteness effects on solutions of the sine-Gordon equation are particularly relevant. There are many different ways in which to generate a spatially discretized partial difference equation for the sine-Gordon equation and at present there are no known exact solutions corresponding to any of these. Each discretization corresponds to a different model by which the series of discrete junctions on the transmission line interact. Once a particular discretization is assumed, the corresponding partial difference equation must be solved numerically. Particular discretizations for some nonlinear partial differential equations other than the sine-Gordon equation are known which can be solved exactly by the inverse scattering transform (see Ref. 21 and references therein). Recently, Ablowitz and Ladik have explained how to find and solve a class of nonlinear partial difference equations which converge to an exactly solvable nonlinear equation in the continuum limit using the "inverse-scattering" technique.[22] Moreover, they have discovered important features that their solutions have in common and can thus characterize the discretizations which admit such exact solutions.

The purpose of this paper is fourfold. First, we examine the effects of discreteness on the ability of the chain to support propagating soliton solutions. Second, we complement the numerical work already done[13-15] on the perturbed sine-Gordon system by verifying the qualitative behavior of the two-point impulsive force and model spatial impurity perturbations and by establishing limits of validity of the linear perturbation theory described in I. Third we demonstrate the wave and particle aspects of the nonlinear soliton solution. Fourth, we suggest applications of the above two types of perturbation to the propagation of a quantum of flux along a Josephson-junction transmission line.

Briefly the results for single-soliton propagation we have found are as follows: on the discrete transmission line soliton modes can couple strongly to the continuum excitations. This means that there is a damping and pinning mechanism which resists the free propagation of solitons possible on the continuous line. Moreover, as a function of the coefficient of the nonlinear term, it is possible to distinguish a coherent regime (small coefficient) in which weakly damped traveling single-soliton solutions are possible and an incoherent regime (large coefficient) in which such solutions are no longer possible. Turning to the analysis of the two impurity perturbations of I, the numerical simulation is of course able to go beyond the bounds of linear perturbation theory. The simulation which was conducted in the coherent or nearly continuous regime agrees quantitatively quite well with the continuous linear perturbation theory and it is possible to estimate limits for the size of the perturbation expansion parameter. Our results support the view that it is mostly possible to regard the single soliton as though it were a deformable extended classical particle obeying Newton's Laws of Motion. Our findings have application to the Josephson-junction transmission line in that they predict a pinning and loss mechanism for flux propagation on a discrete line and they model the effect on the propagation of a flux quantum of applying external transverse electric currents at points across the Josephson junction. It is important to understand the latter effect in order to manipulate quanta of flux, i.e., the "bits" of information in memory and logic devices.

The structure of the paper is as follows. In Sec. II we describe details of the computer simulation. Section III deals with spatial discreteness effects on the propagation of single-soliton solutions. Sections IV and V analyze the external applied force (or model impurity potential) problem and the nonlinear coefficient spatial defect simulation of Ref. 6, respectively. Section VI contains our conclusions.

II. COMPUTER SIMULATION DETAILS

Mathematically the general problem may be stated as follows: we seek the behavior of N-soliton solutions of the nonlinear partial differential equation

$$\frac{\partial^2\phi}{\partial t^2} - C_0^2\frac{\partial^2\phi}{\partial x^2} + \omega_0^2(x)\sin\phi + A f(x) = 0\,, \tag{2.1}$$

where C_0 is the limiting speed of propagation (taken to be unity for convenience) and where $\omega_0(x)$ and $f(x)$ are arbitrary functions of x. The work reported in this paper has been primarily concerned with the single-soliton solutions of (2.1) with ω_0 and f taking the two simple forms considered in I:

$$\omega_0^2(x)=\omega_0^2+a\theta(x);\quad f(x)=0,\quad |a|\ll\omega_0^2, \tag{2.2}$$

where $\theta(x)$ is the Heaviside unit step function or

$$\omega_0^2(x)=\omega_0^2;$$

$$f(x)=\frac{1}{\sqrt{\pi}\,\sigma}\left\{\exp\left[-\left(\frac{x-q-w}{\sigma}\right)^2\right]-\exp\left[-\left(\frac{x-q}{\sigma}\right)^2\right]\right\},\quad \omega_0\sigma\ll 1. \tag{2.3}$$

Solutions of (2.1) were found numerically on a finite interval of length L with boundary conditions either

$$\begin{cases}\phi(0,t)=\phi(L,t)+2\pi n=2\pi m;\quad m,n\in\{0,1\}\\ \dot\phi(0,t)=\dot\phi(L,t)=0,\end{cases} \tag{2.4}$$

or

$$\begin{cases}\phi(0,t)=\phi(L,t)+2\pi n;\quad n\in\{0,1\}\\ \dot\phi(0,t)=\dot\phi(L,t),\end{cases} \tag{2.5}$$

where a dot denotes a time derivative.

The interval $[0,L]$ was discretized into L intervals of unit length and Eq. (2.1) was recast as a system of $2L$ ordinary nonlinear differential equations

$$\frac{d}{dt}\vec{Y}=\vec{F}(t,\vec{Y}), \tag{2.6}$$

where

$$\vec{Y}=\begin{bmatrix}\phi(1,t)\\ \dot\phi(1,t)\\ \phi(2,t)\\ \vdots\\ \dot\phi(L,t)\end{bmatrix}. \tag{2.7}$$

For the particular choice of boundary conditions (2.5), $\vec{F}$ takes the form

$$\vec{F}(t)=\begin{bmatrix}\dot\phi(1)\\ \phi(2)-2\phi(1)+\phi(L)-\omega_0^2(1)\sin\phi(1)-\frac{A\phi(1)}{\pi^{1/2}\sigma}\left\{\exp\left[-\left(\frac{1-q-w}{\sigma}\right)^2\right]-\exp\left[-\left(\frac{L-q}{\sigma}\right)^2\right]\right\}\\ \dot\phi(2)\\ \vdots\\ \phi(1)-2\phi(L)+\phi(L-1)-\omega_0^2(L)\sin\phi(L)-\frac{A\phi(L)}{\pi^{1/2}\sigma}\left\{\exp\left[-\left(\frac{L-q-w}{\sigma}\right)^2\right]-\exp\left[-\left(\frac{L-q}{\sigma}\right)^2\right]\right\}\end{bmatrix}. \tag{2.8}$$

A partial difference equation models an actual crystal lattice more realistically than does the original continuum equation. The particular discretization (2.8) corresponds to a chain of particles, each connected to its nearest neighbors only by springs with a uniform linear restoring force. Details of discretization in nonlinear problems may be more important to the physics than they are in linear problems.[21,23] Ours is certainly not a discretization which has the characteristics of Ref. 22, and thus it does not appear to be solvable analytically.

Equation (2.6), with boundary conditions (2.4) or (2.5) and specified initial conditions $\vec{Y}(t_0)$, was solved using the continuing Hamming predictor-corrector (HPC) technique.[24-28] As initial conditions we can specify a one soliton, two soliton, breather solution, etc.[29,30] To test the ideas of I we concentrate on the first two excitations, namely, single-soliton solutions given by

$$\phi_{(s,\bar s)}=4\tan^{-1}\{\exp[\pm\gamma\omega_0(x-q-\beta t)]\}, \tag{2.9}$$

where s and $\bar s$ refer to solitons and antisolitons, respectively, β is the velocity at which the soliton moves, $\gamma\equiv(1-\beta^2)^{-1/2}$, and q is the center (the point where $\phi=\pi$) of the soliton at time $t=0$, or the two-soliton solution given by

$$\phi_{s\bar s}=4\tan^{-1}[\sinh\gamma\omega_0\beta t/\beta\cosh\gamma\omega_0(x-q)]. \tag{2.10}$$

In order to clarify the concept of the nonlinear soliton solution as a particle consider the continuum solutions (2.9) and (2.10). Strictly these are nonlinear wave solutions defined on the interval $[-\infty,+\infty]$. They are specified by parameters (β,q) and $(\beta_1,\beta_2,q_1,q_2)=(\beta,-\beta,q,q)$ which for $a=A=0$ will be constant for all times. If one chooses to describe that part of the solution which rapidly changes by 2π as a "ϕ particle" then these parameters may be interpreted as the velocities and positions of the ϕ particles at time $t=0$. This prescription succeeds for single solitons but for the two-soliton solution these β's and q's lose their speed and position interpretation (see Fig. 1).

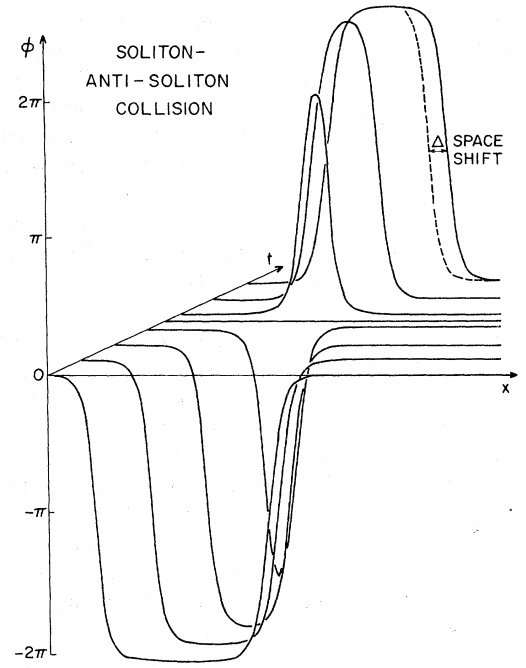

FIG. 1. Simulation of a sine-Gordon soliton-antisoliton collision showing space shift Δ.

When the ϕ particles are far apart they may move with asymptotic speeds β but upon approaching each other they "accelerate." When close together the definition of both ϕ-particle speed and location become ambiguous as the particle and antiparticle annihilate and recreate. Long after annihilation it is possible once again to consider well-separated "particles" with asymptotic speeds β. Viewing the time evolution of the two-soliton solution as a collision event between ϕ particles it is said that ϕ particles upon collision preserve their integrity and suffer only a space (or phase) shift as a result of their interaction.

Now consider the single-soliton solution (for which the ϕ-particle notion is straightforward) in the presence of perturbation of the type of Eqs. (2.2) or (2.3). The nonlinear wave solution may no longer be parametrized by (β, q) independently of time and indeed its analytic form is unknown. In the ϕ-particle interpretation it is possible to describe "interaction" between a particle and external forces so that its speed β becomes a time-dependent variable and its "shape" may vary in time as well. This is the language of perturbation theory and it will be used to give qualitative descriptions of the exact numerical results and to make quantitative comparison with the results of I. The continuum sine-Gordon equation has a number of special properties. For example, it possesses an infinite number of conserved quantities of which total energy and "momentum" are just two and classically its Hamiltonian may be expressed via a canonical transformation[31] as the sum of Hamiltonians corresponding to nonlinear excitations (solitons and breathers) and linear "phonon" excitations. In view of this separability, if an initial state corresponding to a multisoliton solution is specified for the continuum sine-Gordon equation, then at a later time there can be no linear excitations present; linear and nonlinear modes do not couple classically in the continuum theory. Section III considers to what extent this separability remains true when the partial differential equation (2.1) is replaced by the partial differential-difference equation appropriate to a discrete line.

III. DISCRETENESS EFFECTS OF THE SIMULATION

It is always possible, in principle, to make the time steps and the spatial discretization length arbitrarily small so as to find the solutions ϕ corresponding to the continuum equation (2.1) to any desired accuracy. In physical applications, however, minimum distance scales usually occur naturally (e.g., as a lattice constant) and represent a real and sometimes important aspect of the problem. To simulate this situation we chose units in which the lattice constant is unity and studied the behavior of the solutions to (2.1) for different values of ω_0, keeping $a = A = 0$.

The most striking feature of the discrete system is that the allowed solutions, phonons (linearized solutions), breathers, and solitons can couple. The continuum equation has the remarkable conservation property that these excitations have infinite lifetimes and suffer only additive asymptotic phase shifts upon collision. Thus, for example, a traveling one-soliton initial condition leads to a solution describing a traveling one soliton for all time. On the contrary, in the discrete problem, a traveling one-soliton initial condition leads to a solution comprising both a soliton and phonons (commonly referred to in this context as "radiation"). The velocity of the soliton decreases with time while the low-amplitude harmonic oscillations increase in number. The phonons are generated in the wake of the soliton and provide weak viscous damping which draws energy and momentum from the traveling soliton. The residence time of the soliton center in successive unit cells increases as its instantaneous velocity β decreases until β drops below a critical "pinning velocity" β_{pin} when the soliton center is trapped in a particular unit cell. The soliton then executes damped oscillatory motion about the unique stable stationary configuration point in the center of the unit cell until all

the soliton kinetic energy is depleted and it adopts a stationary configuration. Strictly these properties invalidate the conventional terminology "soliton" for our particlelike solutions. We shall continue to use the terms however since no numerical simulation can completely eliminate the continuum-violating errors. Independent of the phonons, the discrete soliton is narrower than the continuum soliton propagating at the same velocity. For example, a soliton launched at $\beta = 0.50$ with $\omega_0 = \frac{1}{2}$ will within four time steps relax into a soliton traveling at $\beta = 0.49$ ($\gamma = 1.15$) with an effective contraction factor $\gamma = 1.23$.

These remarks are conveniently summarized by Fig. 2 which shows an antisoliton launched with an initial velocity considerably below β_{pin} and with $\omega_0 = 1$. Hence the periodic potential is strong and discreteness effects are very pronounced. The soliton can be seen to oscillate with its center between two adjacent "particles" on the chain. During oscillation it changes shape and excites harmonic distortion about 0 and 2π. As the soliton excites more phonons the excursion of its center from the line $(x = 8.5, t, \phi = \pi)$, which constitutes the stable stationary-configuration trajectory, diminishes and it becomes quiescent.

In a lattice the translation symmetry becomes discrete and displacements of the soliton by distances which are not integral multiples of the lattice constant yields solutions propagating at different velocities and with different shapes. The total energy of the system, regardless of discrete or continuous symmetry must remain constant

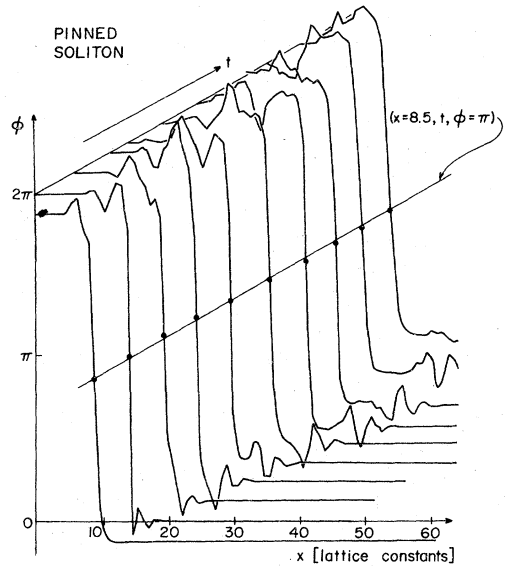

FIG. 2. Simulation of an antisoliton which can not propagate due to the discrete lattice pinning effect.

since the Hamiltonian (discrete or continuous) corresponding to (2.1) has no explicit time dependence. In the lattice, particles must overcome the periodic onsite potential barrier $V(\phi) = \omega_0^2(1 - \cos\phi)$ if the soliton is to propagate along the chain. The lowest soliton potential configuration corresponds to particles being symmetrically placed about $\phi = \pi \bmod(2\pi)$ with no particle at $\phi = \pi$, while the highest soliton potential configuration is again symmetric but with one particle at $\phi = \pi$.

These configurations correspond to highest and lowest propagation kinetic energies, respectively, since the total energy is conserved. This discrete lattice "pinning effect" is found to modulate the velocity of propagation and soliton position sinusoidally with frequency ω_0 and amplitude nearly proportional to ω_0 over the range of ω_0 for which propagating solutions are possible (see below). It is this oscillatory motion of the soliton which steadily creates phonons. The frequency $\omega = \omega_0$ is the lowest frequency of the phonon spectrum in the continuum theory (i.e., $k = 0$ phonon). Clearly, the static soliton configurations to which all travelling solitons eventually decay will be those of lowest potential energy — those whose wall center $(\phi = \pi)$ is to be found midway between two particles of the lattice.

These pinning and oscillatory effects are illustrated by simulation results in Fig. 3 which shows

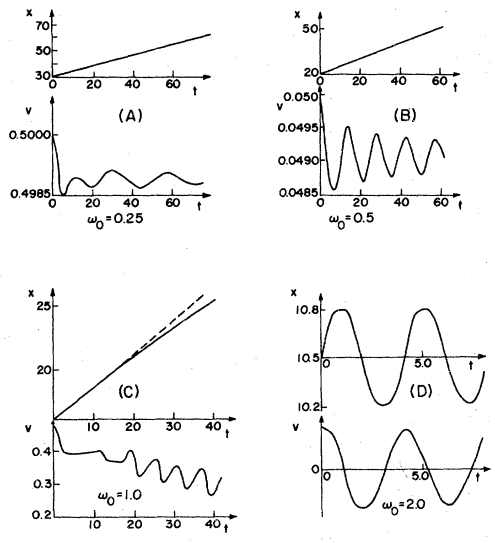

FIG. 3. Plots of the position and velocity of the center of a soliton vs time which illustrate the effect of the lattice on soliton propagation as the magnitude of the nonlinear term ω_0 is increased: (a) $\omega_0 = 0.25$, coherent regime, pinning is negligible; (b) $\omega_0 = 0.50$, coherent regime; (c) $\omega_0 = 1.0$, in zone of transition between coherent and incoherent regimes, pinning effects important; (d) $\omega_0 = 2.0$ incoherent regime: soliton pinned.

the position and velocity of the soliton center as a function of time using four successively larger values of ω_0 after the soliton is launched with a speed $\beta = 0.5$. In all figures there is an apparent "relaxation period" T_R during which the position and velocity behave erratically just after the launch ($t = 0$). This corresponds to the time during which the continuum traveling wave initial conditions relax into the traveling solution appropriate to the discrete problem. Roughly, T_R is one period $2\pi/\omega_0$ of the low-energy phonon mode. In fact an estimate of the relaxation time for the static continuum solution to the stable static discrete solution using a linear stability theory (details at end of this section) shows that this time is far longer than the observed time T_R. The relaxation is due to buildup of oscillatory motion over the whole soliton rather than to a change in shape of the entire soliton.

At times later than T_R a nearly sinusoidal modulation of the soliton commences having a frequency close to ω_0. The time-averaged velocity

$$\bar{v}(t) = \int_{t-\pi/\omega_0}^{t+\pi/\omega_0} v(t')\,dt'$$

suffers an exponential decay that is barely perceptible in the weak on-site potential case, Fig. 3(a) ($\omega_0 = 0.25$), but which is very pronounced in the example of Fig. 3(c) ($\omega_0 = 1.0$). Above $\omega_0 = 1.0, \beta = 0.5$, pinning can easily occur and hence in Fig. 3(d) ($\omega_0 = 2.0$) the soliton center oscillates harmonically between two lattice sites with frequency of nearly ω_0.

A simple estimate for the pinning velocity β_{pin} may be found as follows for $\omega_0 < 1$, where the soliton width spans many lattice sites: consider a traveling soliton whose center moves in an effective periodic potential U with an assumed form $U(x) = \omega_{\text{eff}}^2(1 + \cos 2\pi x)$. For small variations in x about the middle of lattice cell $U(x)$ is nearly harmonic so that ω_{eff}^2, as a function of ω_0, may be determined from a linear stability analysis about the static soliton solution [Eq. (2.9), with $\beta = 0$]. For small ω_0, we expect $\beta_{\text{pin}} \ll 1$ so that γ may be taken to be 1 and nonrelativistic mechanics apply. Thus β_{pin} is the minimum velocity at which the wall can overcome the effective potential barrier of height $2\omega_{\text{eff}}^2$. Using the continuum rest mass of the soliton[30] $M = 8\omega_0$, β_{pin} satisfies

$$\tfrac{1}{2} M \beta_{\text{pin}}^2 \simeq 2\omega_{\text{eff}}^2,$$

so that

$$\beta_{\text{pin}} \simeq \omega_{\text{eff}}/(2\omega_0)^{1/2}. \tag{3.1}$$

Two regimes of the discrete solutions to (2.1) may be defined by the relative strength of the elastic strain term $\partial^2\phi/\partial x^2$ and the on-site force term $\omega_0^2 \sin\phi$. Let a_0 and C_0 be the lattice constant and the limiting speed of propagation for the ϕ particles, respectively (which we have assumed to have values of unity). When the strains dominate and $\omega_0 \ll C_0/a_0$, one is in the "coherent" or "nearly continuous" limit where the discrete solutions propagate coherently as much as the continuum solutions [for example, Eq. (2.9)]. When $\omega_0 \gg C_0/a_0$ the on-site potential completely dominates and one is in the "incoherent" or "discrete" limit where propagating coherent solutions do not occur since the particles are effectively decoupled. Incoherent static solutions consist of ϕ particles distributed randomly along the chain at $\phi = 0 \bmod(2\pi)$; as we shall see the pinning barrier becomes infinite so that there are no moving solitons! Also, we can note from Eq. (2.9) that as $\omega_0 \to \infty$, the continuum soliton width $\lambda \equiv 2C_0/\omega_0$ becomes far smaller than the lattice constant a_0 and the concept of a smooth localized traveling wave solution (soliton) breaks down. The simulations which are reported here are restricted to the coherent region and all satisfy $\lambda \geq 2a_0$.

In order to test the stability of using the continuum result Eq. (2.9) as an initial condition for the discrete simulation and to measure the ω_{eff} of the effective resisting potential $U(x)$ the following linear perturbation analysis was performed (cf. I). Let the solution to the pure discrete sine-Gordon equation ($A = a = 0$) be

$$\phi_i = \phi_i^{(0)} + f_i, \tag{3.2}$$

where $\phi_i^{(0)}$ is either the discretized version of (2.9) or the true minimum-energy static solution of the sine-Gordon equation (obtained numerically), and where f_i is a small discrete-valued function whose time dependence is given by $\sin(\omega t)$. Substituting Eq. (3.1) in the discretized sine-Gordon equation results in the following linearized equation for the f_i:

$$\omega^2 f_i = \sum_{j=1}^{L} D_{ij} f_j, \tag{3.3}$$

where

$$D_{ij} = -\delta_{j,i+1} - \delta_{j,i-1} + \delta_{i,j}(2 + \omega_0^2 \cos\phi_i^{(0)}). \tag{3.4}$$

Solving for the eigenvalues ω^2 of (3.3) requires finding the eigenvalues of the dynamical matrix D. This was done numerically and the results are plotted in Fig. 4. Only the lowest two frequencies are plotted as a function of ω_0 since the remainder are above $\omega = \omega_0$, corresponding to the phonon continuum, and differ little from one another. Note that for the continuum $\phi^{(0)}$, ω^2 is negative for $\omega_0^2 \lesssim 1.1$ reaching a minimum value of $\omega^2 = -0.015$ for $\omega_0 = 1$. This indicates that the continuum initial condition relaxes to the discrete configuration with an approximate characteristic time of more than 8 time units. Since the adjustment observed between

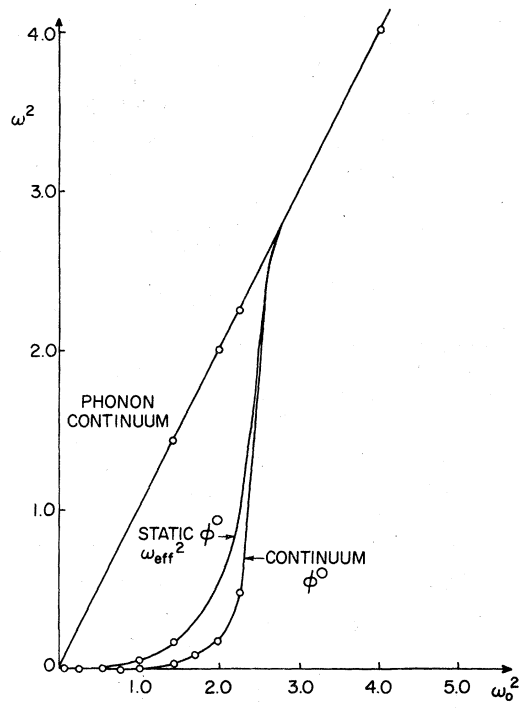

FIG. 4. Plot of the lowest eigenvalue ω^2 of the dynamical matrix Eq. (3.4) vs ω_0 for the two cases: (i) ϕ is the static discrete solution and (ii) ϕ is the static continuum solution. Note for the latter that the lowest eigenvalue is negative for $\omega_0 \lesssim 1.1$. Also shown is the phonon continuum corresponding to both cases.

continuum and discrete solutions is very small, the continuum initial condition is completely adequate for an accurate simulation. For $\omega_0 > 1$ the frequency ω rises rapidly to ω_0 because as ω_0 becomes larger than 1, the soliton width $\lambda = 2C_0/\omega_0$ becomes smaller than the lattice constant a_0 and the soliton approaches the function $\phi^{(0)}(x) \simeq 2\pi\theta\ (x-q)$. Long-wavelength linear oscillations about this function will be exactly those of frequency ω_0.

Consider now the curve for the static $\phi^{(0)}$. It is always positive indicating that the static solution is stable. The frequency $\omega = \omega_{eff}$ is the frequency of low-amplitude oscillations of the soliton about its static configuration. ω_{eff} increases to a value equal to ω_0. The rapid increase appears to begin near $\omega_0 \simeq C_0/a_0$, i.e., when $\lambda \simeq 2a_0$.

In the continuum theory the lowest eigenfrequency ω is identically zero corresponding to a free-translation mode.[6] Results similar to ours but for the nonlinear Klein-Gordon equation with ϕ^4 potential have been obtained by Aubry.[32]

These results have significant consequences for the design of Josephson-junction memory and logic devices. Consider a discrete lossless transmission line whose equivalent circuit has unit spacing a_0, series inductance per unit length L, a shunt capacitance per unit length C, and a maximum Josephson current per unit length J_c. Then in terms of these constants and the flux quantum $\Phi_0 = h/2e$, the constants in Eq. (2.1) correspond to[13]

$$\omega_0^2 = 2\pi J_c/\Phi_0 C \quad \text{and} \quad C_0^2 = 1/LC\,. \tag{3.5}$$

Hence $\lambda = 2C_0/\omega_0 = (2\Phi_0/\pi L J_0)^{1/2}$. The ideal situation for flux propagation with weak damping is $\lambda \gg a_0$. However, high-density requirements force λ to be close to a_0. Note that this discreteness damping occurs in addition to resistive loss mechanisms and must be considered in power requirements for moving fluxons and in noise (or linear oscillation) generation. The effect of applying an external current transverse to the Josephson junction on propagating flux quanta will be described in Sec. IV.

IV. MODEL IMPURITY POTENTIAL SIMULATION

In this section we consider the effect of an impurity (or external) force of the form of Eq. (2.3) when the characteristic frequency ω_0 is constant ($a = 0$). In I a perturbation theory in the small parameter $\epsilon \equiv A/\omega_0\beta^2$ is used to calculate (to first order in ϵ) expressions for the delay distance Δ and the speed β_1 of the soliton when its center is located in the middle of the impurity region. Assuming that the collision takes place at $t = 0$, and using the same sign conventions for A as in I, the results are

$$\Delta \equiv \lim_{t\to\infty}[x(t) - x(-t) - 2t\beta(-t)] \tag{4.1}$$

$$= \tfrac{1}{4}\pi A w/\beta^2\gamma^3\,, \tag{4.2}$$

$$\beta_1 = \frac{\beta - (A/\omega_0\beta\gamma)\tan^{-1}\exp(\frac{1}{2}w\omega_0)}{1 - (A/\omega_0\gamma)\tan^{-1}\exp(\frac{1}{2}w\omega_0)}\,, \tag{4.3}$$

$$\cong \frac{\beta - A\pi/2\omega_0\beta\gamma}{1 - A\pi/2\omega_0\gamma} \quad \text{for } \tfrac{1}{2}\omega_0 w \gg 1\,. \tag{4.4}$$

Results such as Eqs. (4.2) and (4.4) are given in terms of the variables and parameters of Eq. (2.1) rather than in the dimensionless quantities introduced in I. For convenience, Table I compares the variable and parameter systems.

The actual precision of results (4.2) and (4.4) is difficult to establish since the perturbation calculation was not carried to higher orders in ϵ. Any errors quoted below for (4.2) and (4.4) will refer only to the uncertainty due to empirically established parameters in the numerical simulation.

Reference 6 also displays the perturbation theory results for the deviation of the soliton from the asymptotic soliton shape. This deviation was calculated to first order in ϵ using unrelaxed initial conditions (contour deformations); even in the absence of the soliton, the initial distortion of Fig. 3(a) of

TABLE I. Dictionary of variables and parameters used in this paper and in Ref. 6.

Reference 6	This paper
τ	$t=\tau/\omega_0$
z	$x=zC_0/\omega_0$
α Sec. III of Ref. 6	$A=\alpha\omega_0$
z_0	$w=2z_0/\omega_0$
$\epsilon=\alpha/\beta^2$	$\epsilon=A/\omega_0\beta^2$
α Sec. V of Ref. 6	$a=\alpha\omega_0^2$

Ref. 33 would relax to Fig. 4 of Ref. 33. What one sees in the sequence [Figs. 3(a)–3(g) of Ref. 33] is this particular choice of initial conditions undergoing a complicated collision and relaxation process. As the impurity approaches the soliton it is trying to relax from its initial shape to the stable shape of Fig. 4 of Ref. 33. Before the soliton completes this relaxation, it collides and distorts in the immediate vicinity of the impurity. Asymptotically after the collision with the impurity, it should emerge with the same shape if a fully relaxed initial shape was used. Figure 5 shows the difference $Q(x)$ (solid line) between the simulated solution and the continuum free soliton solution for the same choice of parameters as Fig. 3 of Ref. 33 at three times which correspond to Figs. 3(a), 3(f), and 3(g) of Ref. 33. We indeed observe no significant change in the structure of the solution before and after the collision. When the soliton is inside the impurity, however, this structure disappears into the very low amplitude radiation traveling away from the impurity site.

The dotted line in Fig. 5 represents the linear perturbation continuum solution in the absence of a soliton. Its amplitude is 0.11 rad while the simulation solution has an amplitude of 0.07 rad. The difference in amplitude is of order α^2 ($\alpha=0.2$), so that the perturbation-shape prediction and the simulation result agree. As we shall see below, the perturbation theory of I also provides adequate agreement for the three other major particle characteristics: space shifts, velocities, and critical velocities.

Treating the soliton as though it were a classical ϕ particle and using simply the ideas of energy conservation (see also Refs. 13–16) it was shown that a soliton can be trapped if its speed β is less than

$$\beta_c=\left(1-\left\{1+\frac{A}{2\omega_0}\tan^{-1}\left[\sinh\left(\frac{\omega_0 w}{2}\right)\right]\right\}^{-2}\right)^{1/2}. \quad (4.5)$$

If a particle is trapped, it oscillates in an effective potential. Approximating this potential $V(x)$ at a distance x from the center of the impurity by the energy of a static undeformed free soliton displaced a distance x from the center gives

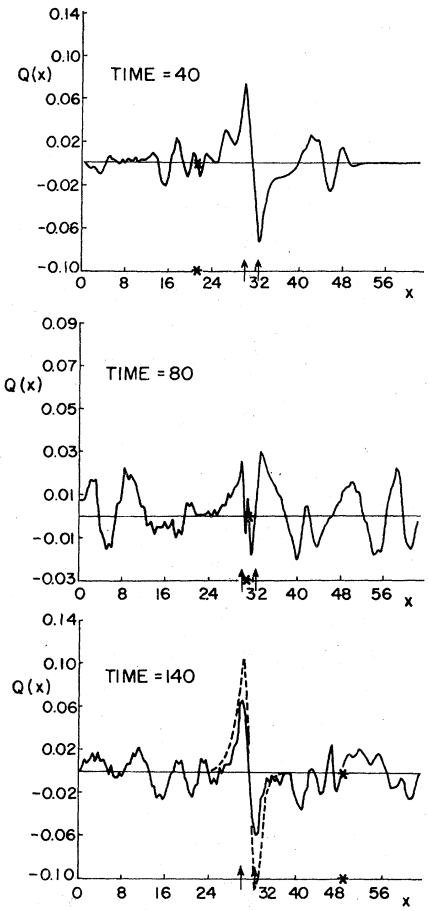

FIG. 5. Plot of the difference $Q(x)$ (solid lines) between the simulated solution and the continuum solution for parameters identical to Fig. 3 of Ref. 33. The dotted line represents the perturbation continuum solution in the absence of a soliton. Asterisks show the location of the center of the soliton while arrows locate the impurity boundaries.

$$V(x)\simeq 4A^2C_0\tan^{-1}\left(\frac{\sinh(\frac{1}{2}w\omega_0)}{\cosh(x\omega_0)}\right) \quad (4.6)$$

as in I (see also Ref. 8).

The oscillatory motion can be easily studied in detail in two different regimes. First if the spatial extent of the soliton is small with respect to the impurity width w, $w\gg\lambda$, the soliton should oscillate harmonically for x sufficiently small and elliptically for slightly larger excursions. The power-series expansion of (4.6) is

$$V(x)=\tfrac{1}{2}M\frac{A}{\omega_0}\tan^{-1}S+\tfrac{1}{2}\frac{S\omega_0^2x^2}{C^2}-\frac{1}{24}\frac{S\omega_0^4}{C^2}\left(\frac{6}{C^2}-1\right)x^4-\frac{1}{720}\frac{S\omega_0^6}{C^2}\left(\frac{120}{C^4}-\frac{56}{C^2}-1\right)x^6+\cdots, \quad (4.7)$$

where

$$M = 8A\omega_0 \quad (C_0 = 1), \tag{4.8}$$

$$C = \cosh(\tfrac{1}{2}\omega_0 w), \tag{4.9}$$

$$S = \sinh(\tfrac{1}{2}\omega_0 w). \tag{4.10}$$

In the second regime, the soliton's extent is much larger than the width of the impurity potential. This suggests that the simple harmonic approximation to the potential V is inadequate and, as verified by simulation, that the potential is distinctly anharmonic. As long as the excursion x does not exceed a maximum (estimated below), the potential V may be truncated after the quartic term and the oscillation will be strongly elliptic. The implicit general result following from Eq. (4.6) can be found in Ref. 33.

Taking as a criterion that the next-higher-order term contributes a correction of <10%, we can define harmonic and quartic domains for the potential (4.7). In the harmonic domain, for all times

$$0 \le |x(t)| \le (1/\omega_0)\{\tfrac{6}{5}[C^2/(C^2-6)]\}^{1/2}. \tag{4.11}$$

The center of the wall is then expected to move according to

$$x(t) \simeq x_0 \sin(\omega t), \tag{4.12}$$

where

$$x_0 \equiv \cosh^{-1}\left(\frac{S}{\tan[\tan^{-1}S - 2(\gamma^*-1)\omega_0/|A|]}\right), \tag{4.13}$$

$$\gamma^* \equiv (1-\beta^{*2})^{-1/2}, \tag{4.14a}$$

$$\beta^* \equiv \beta(x=0), \tag{4.14b}$$

$$\omega \equiv \omega_0 (AS/2\omega_0 C^2)^{1/2}. \tag{4.15}$$

In the quartic domain, for all times

$$0 \le |x(t)| \le \frac{1}{\omega_0}\left(\frac{3C^2(6-C^2)}{C^4+56C^2-120}\right)^{1/2}, \tag{4.16}$$

$$x(t) \approx x_0 \,\mathrm{sn}(\omega t), \tag{4.17}$$

$$x_0 \equiv \frac{1}{\omega_0}\left(\frac{6C^2}{6-C^2}\left\{1-\left[1-2\left(\frac{\omega_0(6-C^2)}{3|A|S}\right)^{1/2}\beta^*\right]^{1/2}\right\}\right)^{1/2} \tag{4.18}$$

$$\omega \equiv \left(\frac{|A|\omega_0 S}{4C^2}\left\{1+\left[1-2\left(\frac{\omega_0(6-C^2)}{3|A|S}\right)^{1/2}\beta^*\right]^{1/2}\right\}\right)^{1/2}, \tag{4.19}$$

where $\mathrm{sn}(\omega t)$ is the Jacobi elliptic function.[34] Note that in the harmonic domain x_0 and ω are independent while they are related in the quartic domain. For small enough x_0 the quartic solution reduces to the harmonic one, but for sufficiently large x_0 the oscillation is strongly nonlinear.

In these simulations the "impurity" force was introduced suddenly at points which were at equal distances from the center of a free traveling soliton. After a relaxation time T_R, the soliton center's oscillation had a nearly constant frequency ω and amplitude x_0. We observed that $T_R \simeq 2\pi/\omega$. The frequency and amplitude were observed to decrease very slowly due to the generation of phonons (see Sec. IV). We find that this slow decrease is consistent with the discrete lattice effects accompanying the choice of model parameters.

Tables II–IV summarize the results for the model impurity simulation, and compare them to the predictions of I. In Table IV, the velocity β^* could only be found indirectly due to the relaxation from the initial conditions. We present two methods of solution, one assuming harmonic motion and the other assuming quartic motion. In the former $\beta^* = x_0^{\mathrm{comp}}\omega^{\mathrm{comp}}$, where x_0^{comp} and ω^{comp} are least-squares fits to the observed amplitude and frequency, respectively, while in the latter β^* is found by solving Eq. (4.19).

In the trapping problem we consider two cases: $\lambda/w \gg 1$ and $\lambda/w \ll 1$. As we have said, for $\lambda/w \ll 1$ the soliton is very narrow compared to the impurity and so should behave as a pointlike particle, i.e., deformation of the soliton from its free shape should have little effect on the motion of the center of the soliton. In the opposite limit $\lambda/w \gg 1$ the soliton is very wide compared to the impurity, and deformations from the free state should be highly localized. On the scale of the soliton extent the potential's nonharmonic components become important. For sufficiently low velocities we assume that the quartic component is the dominant nonharmonic part of the potential. This assumption is supported by the results reported in Table IV.

TABLE II. Comparison of perturbation predictions and simulation observation for space shift and intermediate velocity.

ϵ	Δ	Δ^{comp}	β_1	β_1^{comp}	Model parameters				
					ω_0	$\langle\beta\rangle$	w	A	σ
0.723±0.004	15.02±0.75	9.27±0.54	0.856±0.005	0.694±0.004	$\frac{1}{2}$	0.588±0.001	50.0	$\frac{1}{8}$	1
0.130±0.001	2.16±0.11	1.67±0.08	0.648±0.003	0.614±0.004	$\frac{1}{2}$	0.588±0.001	40.0	0.0225	1

TABLE III. Critical velocity determination.

β_c	β_c^{comp}	Parameters ω_0	A	w	σ
0.500	0.489±0.002	$\frac{1}{2}$	0.1527	5.0	1.0
0.530	0.521±0.002	$\frac{1}{4}$	0.1527	5.0	1.0

The qualitative aspects of the simulation are summarized by Figs. 6–8. Figure 6 shows the space-shift effect of a collision of an antisoliton with the second model impurity of Table V. Here the amplitude A of the impurity is so small that shape change due to the impurity is imperceptible. Most of the velocity and soliton shape change occurs when the center of the soliton coincides with the centers of the δ impurities. Figure 7 demonstrates the trapping of a freely moving soliton at the time $t=0$ by a strong model impurity turned on at that instant. One sees the deformation of the free soliton by the δ-function forces and the transients that are generated by their sudden introduction. Examining the displacements of the soliton center (·) from the center of the impurity, the oscillating behavior is evident. This flexural behavior is what is meant by the deformability of the ϕ particle. While the actual shape of the soliton is not that of the continuum equation (2.9), due to the presence of the external forces or impurity, the potential experienced by the ϕ particle is evidently remarkably close to the $V(x)$ calculated using Eq. (2.9).

Figure 8 gives the position of the center of the soliton as a function of time for the two cases reported in Table IV. Figure 8(a) corresponds to the soliton being very narrow compared to the impurity width, and the position (solid line) is nearly a harmonic function of time. The dotted line gives a sine curve with the computed amplitude and frequency. During the first half-period the ϕ particle may experience a larger excursion since the effect of the δ-function potential is not fully felt until the chain relaxes to a stable distortion after the external force is turned on. Figure 8(b) shows the position when the soliton width is larger than the impurity width. Initially the amplitude is large again due to the fact that the external force is introduced suddenly. Ultimately it settles down to an almost elliptic oscillation in time since its maximum amplitude does not exceed the excursion for which x^6 corrections to $V(x)$ are important [see Eq. (4.16)].

These simulations contribute to an understanding of flux manipulation along a continuous Josephson-junction transmission line. The external force modeled by (2.3) corresponds to a pair of applied infinitely narrow current pulses in opposite direc-

TABLE IV. Oscillating soliton trapped by an impurity.

Calculation	Theory x_0	Simul. x_0^{comp}	Theory ω	Simul. ω^{comp}	ω_0	β^*	A	w	σ	λ/w	Comments
Harmonic	0.30±0.03	0.65±0.05	0.324±0.03	0.29±0.02	$\frac{1}{2}$	0.19 ±0.03	0.86	3.0	1	1.3	Particle is so extended that it should behave anharmonically
Quartic	0.62±0.06	0.65±0.05	0.29 ±0.03	0.29±0.02	$\frac{1}{2}$	0.21 ±0.03	0.86	3.0	1	1.3	Quartic works better than harmonic
Harmonic	1.25±0.15	1.05±0.10	0.11 ±0.01	0.14±0.01	1.0	0.146±0.02	1.8	10.0	1	0.19	Particle is pointlike; harmonic approximation sufficient
Quartic	2.7 ±0.5	1.05±0.10	0.14 ±0.02	0.14±0.01	1.0	0.17 ±0.02	1.8	10.0	1	0.19	

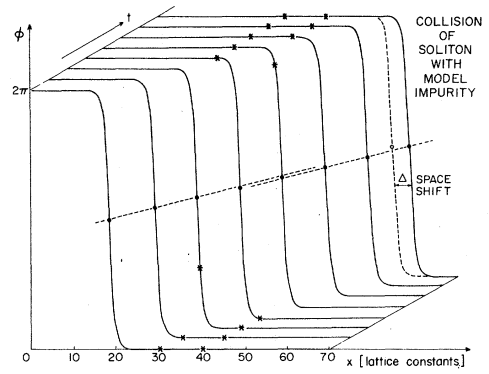

FIG. 6. Simulation of a collision between an antisoliton and the model impurity of Eq. (2.3). The center of the soliton is indicated by a dot while asterisks mark the location of the applied force.

tions, applied a distance w apart with magnitude $j_{app}=\Phi_0 CA/2\pi$. Applying pulses singly has the effect of speeding up or slowing down the flux quantum, depending on the sign of j_{app}. Flux quanta incident on a repulsive pulse will be reflected unless the flux is traveling above a critical velocity. Applying currents in equal and opposite pairs may trap flux. Turning off one of the currents would force the soliton to move in a preferred direction. The consequences for manipulation of "bits," using the flux quanta to carry the information, are intriguing.[18,19] With respect to low-loss lines the present study allows one to establish applied current requirements and the extent to which trapped flux quanta can oscillate, generate noise, and couple with ambient alternating current fields.

V. CHARACTERISTIC FREQUENCY DEFECT

This section is concerned with the characteristic frequency spatial defect of Eq. (2.2) in the absence of external forces ($A=0$). The results are appropriate to physical situations of soliton transmission from one medium characterized by ω_0^2 to another medium characterized by ω_0^2+a. Again using perturbation theory in the small parameter a, Ref. I finds that the asymptotic soliton speed β' long after crossing the defect is related to the incident velocity β [as long as $\beta>\beta_c\equiv a/(1+a)$] by

$$\beta' \simeq \beta + \tfrac{1}{2}a(1/\beta - \beta)\,. \tag{5.1}$$

Using classical energy-conservation arguments, β' is given by

$$\beta'^2 = \beta^2(1 - a/\beta^2 + a)\,, \tag{5.2}$$

agreeing with Eq. (5.1) to first order in a. Not only will the speed change to β' but also the shape of the soliton should adjust to reflect the new characteristic width. The perturbation theory also predicts that there will be a transient contribution to the soliton solution localized near the step which vanishes when the soliton is asymptotically far from the step defect. Finally, classical energy conservation arguments dictate that there should be a critical velocity β_c below which a soliton will be reflected by the step

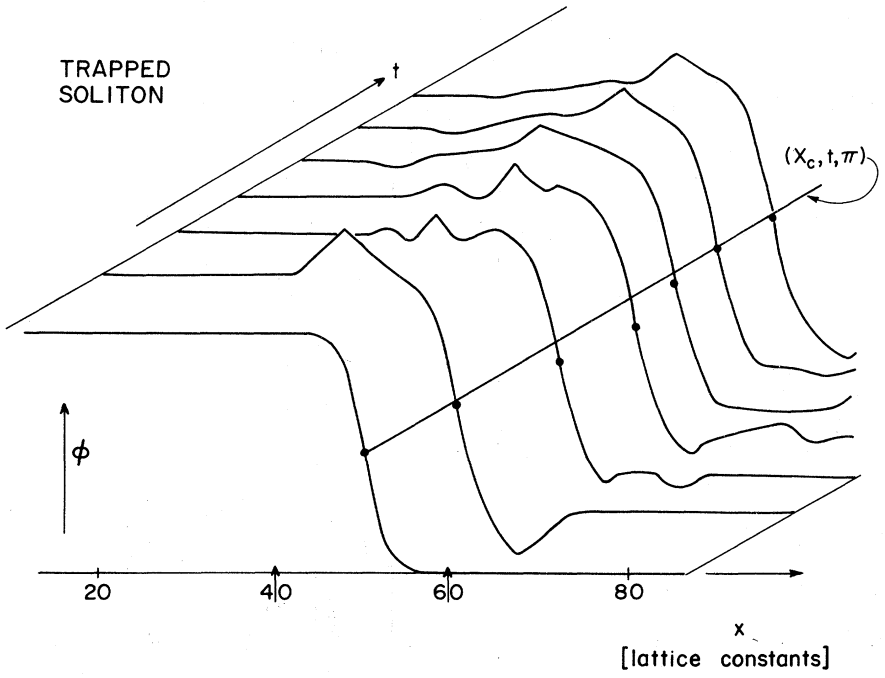

FIG. 7. Simulation showing an antisoliton trapped by an impurity. Dots show the center of the antisoliton and the two arrows show the location of the two edges of the impurity at time $t=0$ when the impurity is suddenly introduced. The line shows the center of the impurity as the collision evolves.

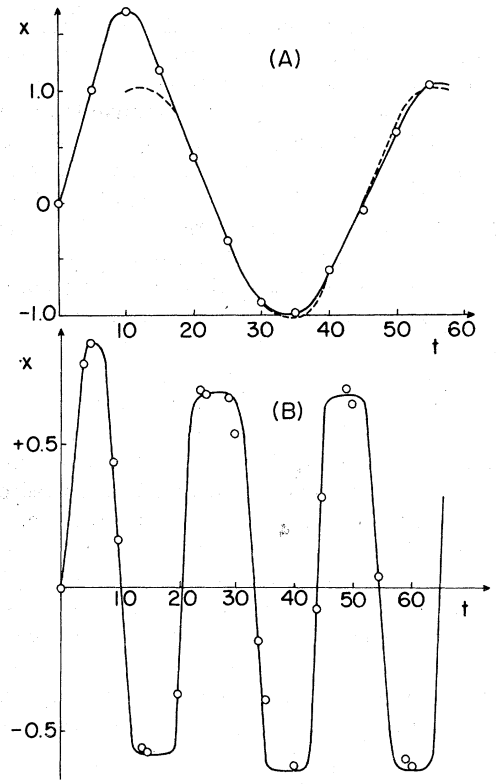

FIG. 8. Plots of the position of the center of the soliton as a function of time in two limits. (a) The soliton is narrow compared to the impurity width; (b) The soliton is wide compared to the impurity width.

$$\beta_c = a/(1+a)\,. \tag{5.3}$$

If the step in ω_0^2 has finite width w then it is predicted that a soliton will be phase shifted by

$$\Delta = a w/4\beta^2\gamma^3\omega_0\,, \tag{5.4}$$

or, if a has the correct sign, the step is high enough and the incident velocity low enough, then the soliton can become trapped in a manner analogous to that discussed in Sec. IV. The results presented in Table VI show that predictions of Eqs. (5.2), (5.3), and (5.4) compare well with the simulation observations.

That the computed velocity change is larger than the predicted change is due largely to the fact phonons (or radiation) are created by collision with the step and since energy must be conserved the velocity of the transmitted soliton is lower than predicted. Discrete lattice effects also add to the slowing down of the transmitted soliton, as described in Sec. III.

Quantitative observations shown in graphs of $\phi(x,t)$ at the left of Fig. 9 illustrate the collision of an antisoliton with a small step. The right-hand graphs in Fig. 9 depict the time-dependent difference $Q(x,t)$ between the simulated soliton and the free soliton. While it is not evident from the plots, after the collision the shape of the soliton broadens to correspond to the longer characteristic width. Also Fig. 9 shows that as the soliton approaches the step defect, at time = 20, large-amplitude linear disturbances are generated at the tail of the soliton. After the collision, at time = 40, and after the large-amplitude disturbances cease to be created and begin to separate into two broadening pulses: one a large transmitted pulse propagating in the direction of the soliton, and the other a small reflected pulse traveling in the opposite direction. Reference 6 predicts that relatively large time-dependent linear disturbance generated by the passage of the soliton over the step is localized at the step and moreover is only appreciable in size when the soliton is in the immediate vicinity of the step.

From the point of view of a lossless transmission line, material defects which vary ω_0^2 spatially constitute possible new pinning mechanisms (see also Ref. 15), modify propagational properties and generate noise in the circuit. Again, this kind of defect is an interesting model for the effect of interfaces (e.g., grain boundaries) on magnetic wall propagation.[2]

TABLE V. Choice of model parameters for simulations of Secs. II and IV.

Parameter	Value	Comments
ω_0	$\frac{1}{4}$	Discrete lattice effects negligible (see Sec. III)
L	200	Spatial period of system
δ	0.001	Maximum truncation error allowed
Δt	0.25	Maximum time step size
β	$0.5 \pm 0.1\%$	Launch and asymptotic velocity

TABLE VI. Comparison of values of quantities predicted by Ref. 6 to those observed in a simulation with $a = \frac{1}{4}$ and $\omega_0 = \frac{1}{2}$. Except for the critical velocity β_c measurement, the free (initial) speed $\beta_i = \frac{1}{2}$. β_T is the asymptotic transmitted velocity and Δ is the space shift corresponding to $w = 20.0$.

Quantity	Prediction of Ref. 6	Observed value
$\beta_i - \beta_T$	0.073 ± 0.003	0.091 ± 0.004
β_c	0.200	0.197 ± 0.002
Δ	3.56 ± 0.17	3.71 ± 0.20

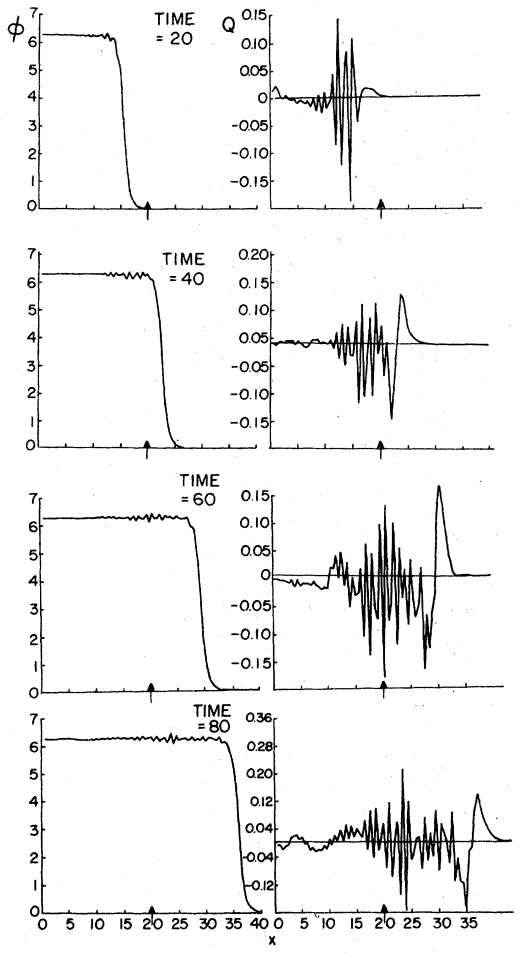

FIG. 9. Collision of a soliton with a step model characteristic frequency defect located at arrow.

VI. CONCLUSIONS

In the preceding sections we have presented the results of a general, accurate, and flexible numerical simulation program. These results provide valuable insights, both quantitative and qualitative, to the problem of lossless soliton propagation on a discrete or continuous chain governed by the sine-Gordon equation with spatially varying coefficients or an external forcing term. Numerical simulations in general can provide a "controlled experiment" in which multisoliton, "breather," and other initial conditions can be observed to interact with arbitrarily specified forces or with each other. Specifically, numerical simulations are extremely valuable in verifying the results of perturbation schemes, in establishing limits to their range of validity, and in providing models for experimental phenomena. An example of the latter kind of application is afforded by the propagation of magnetic flux along a Josephson-junction transmission line.

The study of discreteness effects reveals that unlike the situation for continuous transmission lines, soliton, and linear (or 'phonon') modes can be coupled quite strongly. For ω_0 small compared to C_0/a_0, this leads to a weak damping for soliton propagation and the possibility of a traveling soliton becoming pinned if its speed falls below a "pinning speed." When $\omega_0 \gtrsim C_0/a_0$, coherently propagating solitons are no longer possible.

Simulations of the effects of perturbations of the form (2.2) and (2.3) (as treated in I) on single solitons indicated that so long as the perturbation parameter ϵ did not exceed about 0.1, the predictions in I for space shifts and velocities were accurate to better than 25%. The ansatz of I in which solitons are treated as classical ϕ particles obeying Newton's laws and subsequent predictions based on this idea were found to be in excellent agreement with the simulation. However the predictions concerning the form of the linearly perturbed solution shape, radiation, etc., did not agree adequately with observations. This is due to the fact that the perturbation-shape calculations were performed with unphysical initial conditions.

One of the many contexts in which Eq. (2.1) appears is in the flux propagation along an ideal Josephson-junction transmission line and this example has been used to illustrate some of the possible applications of the work in I and this simulation. We have shown that even on lossless lines there can be damping, pinning, and noise generation due to discreteness effects. Model forces such as (2.3) can accelerate flux quanta and space shift or trap them just as conducting filaments transverse to the Josephson-junction may be used to manipulate bits of information. The present study also demonstrates that spatial changes or defects in transmission line properties can provide another barrier to free flux propagation and a further source of noise generation. Corresponding applications to other physical contexts (e.g., model magnetic domain walls[2] and ϕ particles in certain linear-chain conductors[4]) will be described in detail elsewhere.

ACKNOWLEDGMENTS

We have benefited greatly from correspondence and discussions with M. B. Fogel, M. J. Ablowitz, F. Y. F. Chu, J. Corones, T. A. Fulton, D. J. Kaup, and A. C. Newell.

*Work supported in part by the ERDA under Contract No. EY-76-5-02-3161.000 (Technical Report No. 52) and also by the Cornell Materials Science Center (Report No. 2750).

†Present address: Dept. of Physics, University of Southern California, University Park, Los Angeles, Calif. 90007.

‡Present address: Physics Dept., Queen Mary College, Mile End Rd., London E1 4NS, England.

[1]For a review, see A. C. Scott, F. Y. F. Chu, and D. W. McLaughlin, Proc. IEEE 61, 1443 (1973); and A. Barone, F. Esposito, C. J. Magee, and A. C. Scott, Riv. Nuovo Cimento 1, 227 (1971).

[2]U. Enz, Helv. Phys. Acta 37, 245 (1964).

[3]A. Seeger, H. Donth, and A. Kochendörfer, Z. Phys. 134, 173 (1953).

[4]M. J. Rice, A. R. Bishop, J. A. Krumhansl, and S. E. Trullinger, Phys. Rev. Lett. 36, 432 (1976).

[5]A. C. Scott, *Active and Nonlinear Wave Propagation in Electronics* (Wiley-Interscience, New York, 1970).

[6]M. B. Fogel, S. E. Trullinger, A. R. Bishop, and J. A. Krumhansl, Phys. Rev. Lett. 36, 1411 (1976), hereafter denoted I in text.

[7]See D. J. Kaup, Siam J. Appl. Math. 31, 121 (1976); A. C. Newell, in *Soliton*, edited by R. Bullough and P. Caudry (Springer, Berlin, 1967).

[8]D. J. Kaup and A. C. Newell (unpublished).

[9]D. J. Kaup and A. C. Newell (unpublished).

[10]J. P. Keener and D. W. McLaughlin, Phys. Rev. A (to be published).

[11]A. C. Scott, F. Y. F. Chu, and S. A. Reible, J. Appl. Phys. 47, 3272 (1976).

[12]G. B. Whitham, *Linear and Nonlinear Waves* (Wiley-Interscience, New York, 1974).

[13]K. Nakajima, T. Yamashita, and Y. Onodera, J. Appl. Phys. 45, 3141 (1974).

[14]K. Nakajima, Y. Onodera, T. Nakamura, and R. Sato, J. Appl. Phys. 45, 4095 (1974).

[15]K. Nakajima, Y. Sawada, and Y. Onodera, J. Appl. Phys. 46, 5272 (1975).

[16]M. J. Ablowitz, M. D. Kruskal, and J. F. Ladik (unpublished).

[17]T. A. Fulton and L. N. Dunkleberger, Appl. Phys. Lett. 22, 232 (1973).

[18]T. A. Fulton, R. C. Dynes, and P. W. Anderson, Proc. IEEE 61, 28 (1973).

[19]K. Nakajima, Y. Onodera, and Y. Ogawa, J. Appl. Phys. 47, 1620 (1976).

[20]P. Guéret, IEEE Mag. 11, 751 (1975).

[21]M. J. Ablowitz and J. F. Ladik, J. Math. Phys. 16, 598 (1975).

[22]M. J. Ablowitz and J. F. Lakik, Stud. in Appl. Math. 55, 213 (1976).

[23]R. M. May, Nature 261, 459 (1976).

[24]A. Ralston, Math. Comput. 16, 431 (1962).

[25]P. D. Ritger and N. J. Rose, *Differential Equations with Applications* (McGraw-Hill, New York, 1968), Chap. 12.

[26]R. W. Hamming, *Numerical Methods for Scientists and Engineers* (McGraw-Hill, New York, 1962).

[27]A. Ralston, *A First Course in Numerical Analysis* (McGraw-Hill, New York, 1965).

[28]Details of the numerical techniques used and the checks of the computer code performed are available from the authors upon request.

[29]R. F. Dashen, B. Hasslacher, and André Neveu, Phys. Rev. D 10, 4130 (1974).

[30]J. Rubinstein, J. Math. Phys. 11, 258 (1970).

[31]V. E. Korepin and L. D. Faddeev, Theor. Math. Phys. 25, 1039 (1975).

[32]S. Aubry (unpublished)

[33]M. B. Fogel, S. E. Trullinger, A. R. Bishop, and J. A. Krumhansl, Phys. Rev. B 15, 1578 (1977).

[34]M. Abramowitz and I.A. Stegun, *Handbook of Mathematical Functions*, U. S. Department of Commerce, (U.S. GPO, Washington, D. C., 1964).